Appl Phys B (2011) 105:185–190
DOI 10.1007/s00340-011-4708-8

Applied Physics B
Lasers and Optics

A stochastic modeling of morphology formation by optical near-field processes

M. Naruse · T. Kawazoe · T. Yatsui · N. Tate · M. Ohtsu

Received: 11 July 2011 / Published online: 9 September 2011

Abstract We previously reported (S. Yukutake et al. in Appl. Phys. B 99:415, 2010) that by depositing Ag particles on the electrode of a photovoltaic device composed of poly(3-hexylthiophene) (P3HT) and ZnO under light illumination (wavelength $\lambda = 660$ nm) while reversely biasing the P3HT/ZnO p–n junction, a unique granular Ag film was formed. The resultant device generated a photocurrent at wavelengths as long as 670 nm, which is longer than the long-wavelength cutoff λ_c (=570 nm) of P3HT. Such an effect originates from a phonon-assisted process induced by an optical near field. In this paper, we analyze the morphological character of the Ag clusters and build a stochastic model in order to understand the principles behind the self-organized pattern formation process. The modeling includes the geometrical character of the material, its associated optical near fields, and the materials that flow in and out of the system. The model demonstrates behavior consistent with that observed in the experiment. We can see these phenomena as a new kind of self-organized criticality taking account of near-field effects, which will provide an insight into the analysis and design of future nanophotonic devices.

M. Naruse (✉)
National Institute of Information and Communications Technology, 4-2-1 Nukui-kita, Koganei, Tokyo 184-8795, Japan
e-mail: naruse@nict.go.jp

M. Naruse · T. Kawazoe · T. Yatsui · N. Tate · M. Ohtsu
Nanophotonics Research Center, School of Engineering, The University of Tokyo, 2-11-16 Yayoi, Bunkyo-ku, Tokyo 113-8656, Japan

T. Kawazoe · T. Yatsui · N. Tate · M. Ohtsu
Department of Electrical Engineering and Information Systems, School of Engineering, The University of Tokyo, 2-11-16 Yayoi, Bunkyo-ku, Tokyo 113-8656, Japan

1 Introduction

Nanophotonics, which utilizes local interactions involving light and matter on the nanometer scale, enables a wide range of functions, such as energy harvesting [1], energy concentration [2, 3], signal processing [4, 5], transformation [6], nanofabrication [7, 8], and so forth. Studying nanophotonics also gives us a deeper understanding of the primary processes occurring on the nanometer scale both theoretically, as in the dressed photon model [9], and experimentally, as in wave function mapping via near-field spectroscopy [10], among others. In these processes, the shape and size of the nanomaterials, or the material morphology, play a crucial role in providing the designated functions.

We previously reported in [1] that a unique granular Ag film was formed by depositing Ag particles on the electrode of a photovoltaic device composed of poly-(3-hexylthiophene) (P3HT) and ZnO under light illumination (wavelength $\lambda = 660$ nm) while reversely biasing the P3HT/ZnO p–n junction. The resultant device generated a photocurrent at wavelengths as long as 670 nm, which is longer than the long-wavelength cutoff ($\lambda_c = 570$ nm) of P3HT. More detail will be summarized later below. This effect originates from a phonon-assisted process induced by an optical near field, as discussed in [1]. We consider that there are two important associated aspects that should be further addressed: one is to investigate the character of the resultant morphology of the devices, as well as to elucidate the physical mechanism of the pattern formation. The other is to reveal the relationship between the morphological character of the material and its associated optoelectronic performance. In this paper, with a view to revealing the former aspect, we analyzed the morphological character of the Ag clusters and constructed a stochastic model in order to understand the principles behind the formation process involving the geometrical character of the material, its

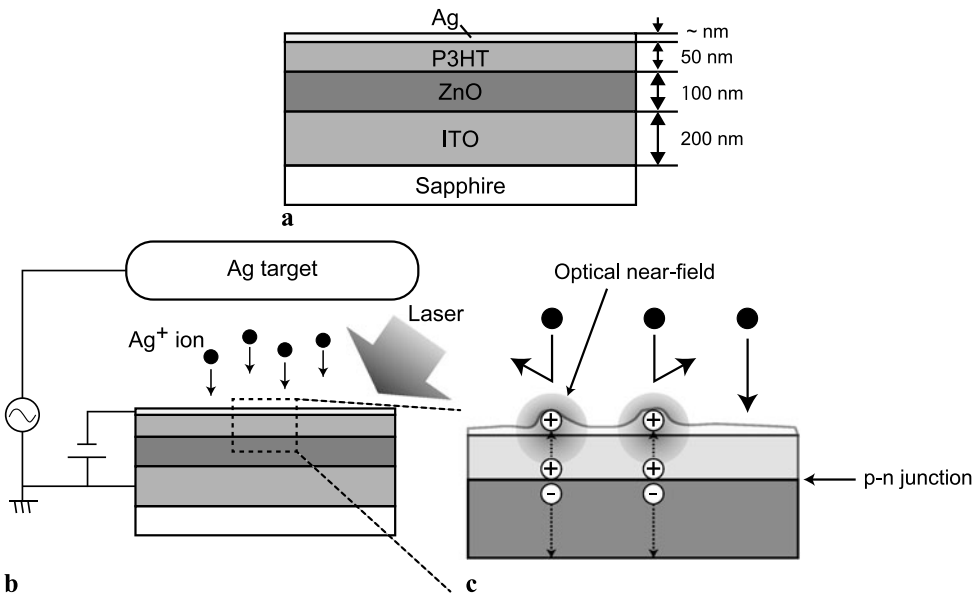

Fig. 1 Cross-sectional structure of the photovoltaic device made of P3HT and ZnO sandwiched by Ag and ITO electrodes. (**b**) A schematic diagram of the Ag sputtering process under laser light irradiation and a reverse-bias DC voltage. (**c**) A close-up of the Ag deposition/repulsion at the surface due to the phonon-assisted optical near-field process

associated optical near fields, and the materials that flow in and out of the system.

The stochastic model described in this paper includes a particle deposition process on the surface while taking account of the repulsion due to the positively charged sputtering particles and the surface of the Ag film, as well as drift processes on the film. The numerical results revealed characteristics consistent with those observed in the previously reported experiment [1] with respect to the incidence patterns of the clusters formed on the surface of the electrode. We can regard this phenomenon as a kind of self-organized criticality [11] that takes into account near-field effects.

This paper is organized as follows. Section 2 reviews the experiment demonstrated in [1] and analyzes the morphology of the surfaces of the fabricated devices. Section 3 demonstrates the stochastic modeling representing the essence of the near-field processes occurring on the nanometer scale and numerical demonstrations. Section 4 concludes the paper.

2 Analysis of the morphology

The device structure analyzed in this paper is summarized as follows [1]. A schematic cross section of the device structure is shown in Fig. 1a. A P3HT layer about 50-nm thick was used as a p-type semiconductor material, and a ZnO film about 200-nm thick was used as an n-type semiconductor. P3HT is commonly used as a hole-conduction component [12]. In the experiment [1], photocurrent generation in a P3HT/ZnO thin film was evaluated at wavelengths longer than the cut-off wavelength of P3HT ($\lambda_c = 570$ nm) which also falls within the wavelength range where the ZnO thin film is transparent (longer than $\lambda = 400$ nm). An ITO film about 200-nm thick and an Ag film a few nanometers thick were used as the two electrodes. In the previously reported experiment [1], thin films of these materials were deposited on a sapphire substrate in series. As a result, a multi-layered film with an area of 30 mm^2 was formed on the sapphire substrate. At the last stage of the fabrication process, Ag was deposited on the Ag thin film, which is the key process in differentiating the resultant performance in terms of photocurrent generation. Figures 1b and 1c schematically illustrate the experimental setup used in [1] and the corresponding processes. Briefly, the Ag is deposited by RF sputtering under light illumination while applying a reverse bias DC voltage, $V_b = -1.5$ V, to the P3HT/ZnO p–n junction. The wavelength of the incident light is 660 nm, longer than the cut-off wavelength of P3HT. Under light illumination, an optical near field is locally generated on the Ag surface, which induces a coherent phonon at the p–n junction, leading to the generation of a virtual exciton–phonon–polariton [1]. This then generates an electron–hole pair at the p–n junction. The electron and holes are separated from each other by the reverse bias voltage. The positive hole is attracted to the Ag film, which makes the Ag film positively charged.

Since the sputtered Ag is positively ionized by passing through the argon plasma or due to the collision of the argon plasma with the Ag target used for RF sputtering [13], these positively ionized Ag particles are repulsed from the positively charged area of the Ag film where the positive holes have been injected, as schematically shown in Fig. 1c. This means that the subsequent deposition of Ag is suppressed in the area where optical near fields are efficiently induced. The processes described here lead to the unique granular structure of the Ag film formed in a self-organized manner, which is the primary focus of the stochastic modeling discussed

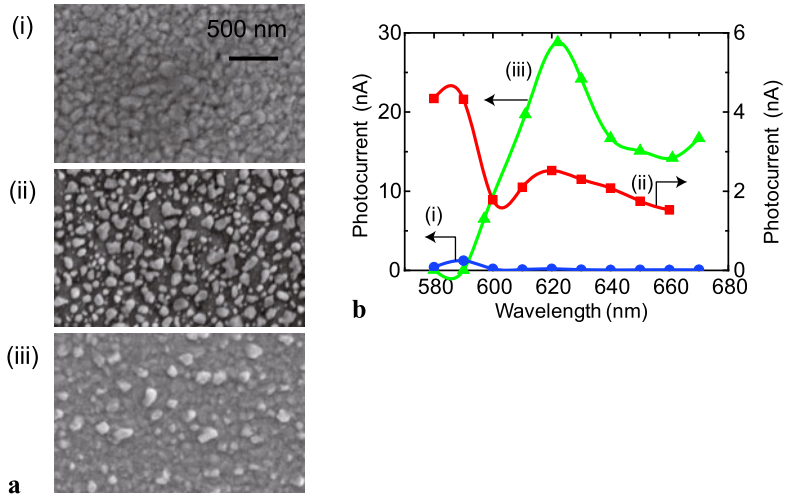

Fig. 2 (**a**) SEM images of the surfaces of the Ag electrodes in three devices fabricated under the following conditions: (**i**) no DC bias ($V_b = 0$), no light irradiation ($P = 0$), (**ii**) $V_b = -1.5$ V, $P = 50$ mW, and (**iii**) $V_b = -1.5$ V, $P = 70$ mW. (**b**) Photocurrent generation in devices (**i**) to (**iii**) in a longer wavelength region where the normal device, case (**i**), exhibited almost no sensitivity, whereas the other two showed evident photocurrent generation

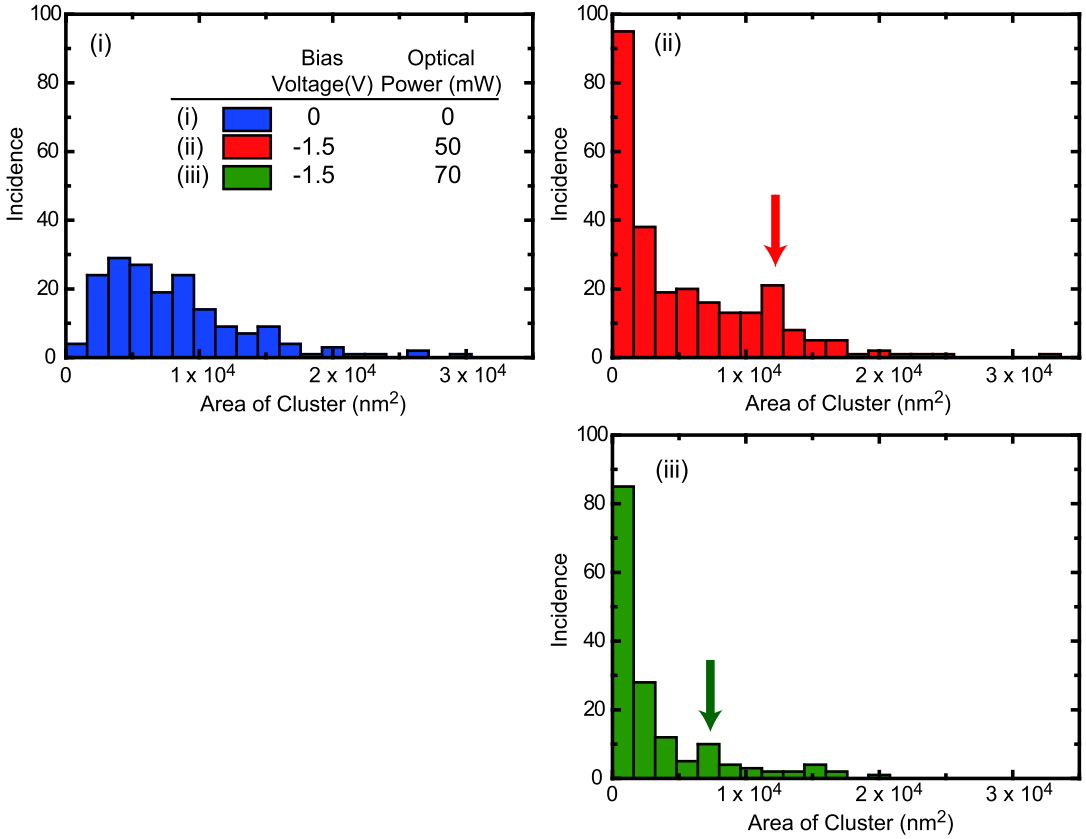

Fig. 3 Incidence patterns of the cluster areas in cases (**i**) to (**iii**) in Fig. 2a

in Sect. 3. Five kinds of devices are discussed in [1], with different combinations of reverse bias voltage and incident light power. In the work described in this paper, we analyzed the following three devices, or cases: (i) $V_b = 0$ and $P = 0$, (ii) $V_b = -1.5$ V and $P = 50$ mW, and (iii) $V_b = -1.5$ V and $P = 70$ mW. Figure 2a shows SEM images of the Ag film surfaces for cases (i)–(iii). It is evident that unique surface morphologies were obtained in cases (ii) and (iii) with the light irradiation. As summarized in Fig. 2b, photocurrents were generated in cases (ii) and (iii) in the longer wavelength range, where case (i) exhibited no response.

Figure 3 represents the incidence pattern as a function of the size of the Ag clusters, obtained by analyzing the SEM images in Fig. 2a. A number of small clusters were observed in cases (ii) and (iii), but some of them were large. Also, as depicted by arrows in Figs. 3(ii) and 3(iii), the incidence

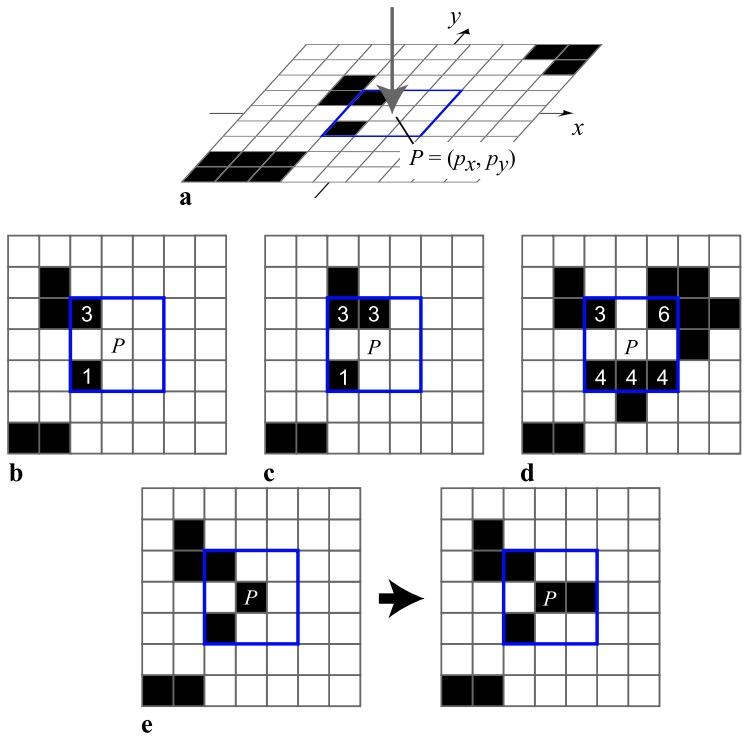

Fig. 4 (**a**) A two-dimensional (2D) grid cell structure used to model the stochastic pattern formation process. (**b–d**) Example to calculate the *pseudo footprint* for a cell P. (**e**) Simulating a drift process when the pseudo footprint at cell P is less than the threshold value but cell P is occupied

showed a local maximum at a particular cluster size. Also note that the maximum appeared at a larger size with lower power light irradiation. On the other hand, case (i) exhibited a different incidence pattern of the cluster area, showing a representative (mode) size of around 5×10^3 nm^2. In other words, we can see evident differences in the surface morphologies between the fabrication processes with and without light irradiation and a reverse DC bias.

3 Stochastic modeling of the morphology formation

3.1 Stochastic modeling

Taking account of the physical processes of the material formation described above, we constructed a simple stochastic model that preserves the essential characteristics. First we consider a two-dimensional (2D) $M \times M$ square grid cell structure Λ_M where a cell, also called a pixel, is specified by $P = (p_x, p_y) \in \Lambda_M$. In each cell, a variable $h(P) \in \{0, 1\}$ is assigned so that areas where the Ag film surface has bumps are represented by $h(P) = 1$, and areas where the surface is flat are represented by $h(P) = 0$. In Fig. 4a, the pixels with $h(P) = 1$ are indicated by black cells, while those with $h(P) = 0$ are indicated by white ones. We simulate the material deposition process as follows.

Initially, we assume a completely flat surface, namely, $h(P) = 0$ for all $P \in \Lambda_M$. First, we randomly choose a cell P in the 2D grid structure and let a particle arrive at P. Second, we determine if the particle successfully lands on a cell or is repulsed, that is, deflected out of the system, by taking account of the positively charged Ag to be sputtered and the holes that could appear on the Ag film surface. We calculate a *pseudo footprint* denoted by Q_P, defined in detail in Sect. 3.2 below, in order to evaluate this effect in the stochastic modeling.

If the calculated value of Q_P is smaller than or equal to a threshold Z, and if the flat surface condition is satisfied ($h(P) = 0$), an arriving particle is able to land on the cell P; that is, $h(P) = 0 \rightarrow h(P) = 1$. In contrast, if Q_P is larger than Z, the arriving particle is deflected outside the system, representing repulsion between the positively charged Ag particle and the positively charged clusters on the surface due to the reverse bias. If Q_P is smaller than or equal to Z but the point P is already occupied ($h(P) = 1$), the arriving particle will sit in a free, randomly chosen neighbor, representing a drift process, of which detail is given in Sect. 3.3.

3.2 Pseudo footprint

The pseudo footprint metric in each square grid cell corresponds to the sum of the areas of its eight neighbors. More precisely, the pseudo footprint at P is given by

$$Q_P = \sum_{i=\{-1,0,1\}, j=\{-1,0,1\}} S_P^{(i,j)}, \tag{1}$$

where $S_P^{(i,j)}$ represents the total number of occupied cells, or area, connected to the cell $(p_x + i, p_y + j)$ either in horizontal (x) or vertical (y) neighbors, as schematically shown

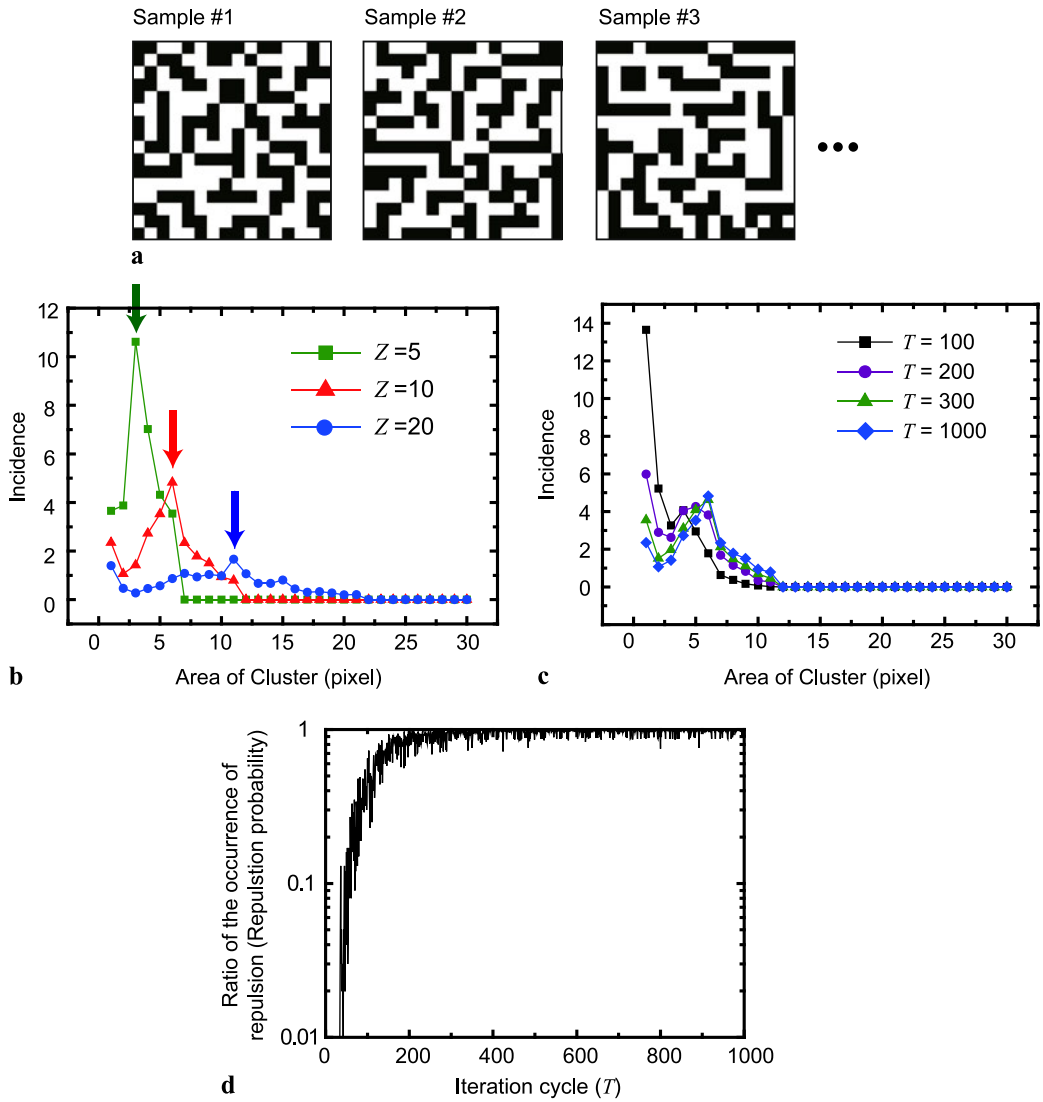

Fig. 5 (**a**) Example of generated patterns via the stochastic modeling. (**b**) Incidence pattern as a function of cluster area, with threshold Z as a parameter. (**c**) Evolution of the incidence pattern of the cluster area as a function of iteration cycle T. (**d**) Evolution of the ratio of the occurrence of repulsion

in Fig. 4a. For example, in the case shown in Fig. 4b, the area of the top-left corner is $S_P^{(-1,+1)} = 3$, and that of the bottom-left one is $S_P^{(-1,-1)} = 1$. Therefore, based on (1), the pseudo footprint is given by $Q_P = S_P^{(-1,+1)} + S_P^{(-1,-1)} = 4$. In another example shown in Fig. 4c, the areas are given by $S_P^{(-1,+1)} = 3$, $S_P^{(0,+1)} = 3$, and $S_P^{(-1,-1)} = 1$, which yields $Q_P = S_P^{(-1,+1)} + S_P^{(0,+1)} + S_P^{(-1,-1)} = 7$. In another example shown in Fig. 4d, $Q_P = \sum_{i,j} S_P^{(i,j)} = 21$.

3.3 Drift

When an arriving Ag particle is not repulsed from the system, but the point P is occupied, the particle lands in a randomly chosen neighboring cell. The left-hand side of Fig. 4e represents one such example where $Q_P = 4$. Suppose that this Q_P is smaller than the threshold Z. Since the point P is occupied, a free neighboring cell is randomly chosen along the x- or y-direction with respect to P. For example, the system is updated as shown in the right-hand side of Fig. 4e, where a newly arriving particle lands to the right of the point P, in other words, $h(p_x + 1, p_y) = 0 \rightarrow h(p_x + 1, p_y) = 1$. Such a rule represents the drift process occurring on the Ag film surface.

3.4 Demonstration

By iteratively applying the stochastic process described above in a repeated manner in T cycles from a flat initial state, a variety of resultant spatial patterns were generated.

They also depended on the threshold Z. By setting the size of the grid to 16 $\times$16 cells, that is, $M = 16$ for the region Λ_M, while setting the threshold at $Z = 10$ and the number of cycles $T = 300$, Fig. 5a represents three examples of the spatial patterns generated in $N = 100$ different trials. We can clearly observe that a variety of resultant patterns were obtained. To examine the statistical properties, the incidence pattern of the mean number of each cluster in N different samples was evaluated, as shown in Fig. 5b where the number of repetition cycles was $T = 1000$. Squares, triangles, and circles respectively represent the incidence of the clusters in the system with different thresholds $Z = 5, 10$, and 20.

The incidence pattern exhibited different characters depending on the threshold value ($Z = 5, 10$, and 20): with smaller Z, the cluster area yielding the local maximum incidence shifted towards a smaller value in Fig. 5b, which agrees with the experimentally observed character shown in Fig. 3 where larger optical light irradiation produced smaller clusters (peaks are indicated by arrows). In other words, higher power light irradiation more likely induces repulsion, leading to a local maximum at a smaller cluster area for the clusters formed on the surface. This supports the physical interpretation that the pseudo footprint appropriately represents the repulsion due to the optical near-field effect. That is to say, the pseudo footprint reflects the positive holes, and the associated optical near field localized around a cluster, or spatial inhomogeneity, is induced.

Figure 5c shows the evolution of the incidence patterns of the cluster sizes as the number of repetitions T increases. We can clearly observe that the peak-like incidence clusters emerge as T increases. Squares, circles, triangles, and diamonds in Fig. 5c respectively show the incidences when T was 100, 200, 300, and 1000. Also, in the initial cycles, the incidence pattern followed a power-law-like statistical property. In considering the steady-state, converged pattern, Fig. 5d characterizes the ratio of the occurrence of repulsion at cycle T among $N = 100$ trials. In other words, it shows the time evolution of the probability of repulsion. The probability increases as the iteration cycle increases; a repulsion probability of 0.8 or higher was observed after the iteration cycle reached around 300. Since the present stochastic model includes a threshold value Z, strictly speaking, it is *not* so-called self-organized criticality [11]. However, as Fig. 5 indicates, a flat surface converges to various kinds of patterns in a self-organized manner while exhibiting common statistical properties, which is a kind of self-organized critical phenomenon due to near-field effects inherent in the stochastic model described above.

4 Conclusion

In summary, in photovoltaic devices made by exploiting an optical phonon-assisted near-field process exhibiting unique photocurrent generation, we analyzed the surface morphology of the Ag electrode of the fabricated devices and constructed a stochastic model to explain the fundamental physical process of the material formation. The numerical simulation results exhibited behavior consistent with the experimental results. The findings reported here will allow us to understand the principles behind the formation process, and to optimize device performance in future.

References

1. S. Yukutake, T. Kawazoe, T. Yatsui, W. Nomura, K. Kitamura, M. Ohtsu, Appl. Phys. B **99**, 415 (2010)
2. T.A. Klar, T. Franzl, A.L. Rogach, J. Feldmann, Adv. Mater. **17**, 769 (2005)
3. M. Naruse, T. Kawazoe, R. Ohta, W. Nomura, M. Ohtsu, Phys. Rev. B **80**, 125325 (2009)
4. M. Naruse, T. Miyazaki, T. Kawazoe, S. Sangu, K. Kobayashi, F. Kubota, M. Ohtsu, IEICE Trans. Electron. **E88-C**, 1817 (2005)
5. C. Pistol, C. Dwyer, A.R. Lebeck, IEEE MICRO **28**, 7 (2008)
6. H. Fujiwara, T. Kawazoe, M. Ohtsu, Appl. Phys. B **98**, 283 (2010)
7. T. Yatsui, K. Hirata, W. Nomura, Y. Tabata, M. Ohtsu, Appl. Phys. B **93**, 55 (2008)
8. S. Yamazaki, T. Yatsui, M. Ohtsu, Appl. Phys. Express **2**, 031004 (2009)
9. M. Ohtsu, K. Kobayashi, T. Kawazoe, T. Yatsui, M. Naruse, *Principles of Nanophotonics* (Taylor & Francis, Boca Raton, 2008)
10. K. Matsuda, T. Saiki, S. Nomura, M. Mihara, Y. Aoyagi, S. Nair, T. Takagahara, Phys. Rev. Lett. **91**, 177401 (2003)
11. P. Bak, C. Tang, K. Wiesenfeld, Phys. Rev. A **38**, 364 (1988)
12. M. Bredol, K. Matras, A. Szatkowski, J. Sanetra, A. Prodi-Schwab, Sol. Energy Mater. Sol. Cells **93**, 662 (2009)
13. J. Joo, J. Vac. Sci. Technol. **18**, 23 (2000)